Editors' Suggestion

Self-Oscillation and Synchronization Transitions in Elastoactive Structures

Ellen Zheng, Martin Brandenbourger⬤, Louis Robinet, Peter Schall, Edan Lerner, and Corentin Coulais⬤

Institute of Physics, Universiteit van Amsterdam, Science Park 904, 1098 XH Amsterdam, Netherlands

The interplay between activity and elasticity often found in active and living systems triggers a plethora of autonomous behaviors ranging from self-assembly and collective motion to actuation. Among these, spontaneous self-oscillations of mechanical structures is perhaps the simplest and most widespread type of nonequilibrium phenomenon. Yet, we lack experimental model systems to investigate the various dynamical phenomena that may appear. Here, we introduce a centimeter-sized model system for one-dimensional elastoactive structures. We show that such structures exhibit flagellar motion when pinned at one end, self-snapping when pinned at two ends, and synchronization when coupled together with a sufficiently stiff link. We further demonstrate that these transitions can be described quantitatively by simple models of coupled pendula with follower forces. Beyond the canonical case considered here, we anticipate our work to open avenues for the understanding and design of the self-organization and response of active biological and synthetic solids, e.g., in higher dimensions and for more intricate geometries.

Introduction.—Active matter systems exhibit exceptional collective, nonequilibrium properties resulting in anomalous dynamical and self-organizing behaviors that challenge conventional laws of statistical mechanics [1–10]. While research has extensively focused on active fluids [2,11]—which consist of collections of individual active particles with no particular geometry [12–16], active solids—which have a well defined reference state and hence exhibit elastic rather than viscous properties at long timescales [17–19]—have been much less studied, despite their potential in mimicking living matter and forming novel active materials [18–20].

Among all kinds of mechanical properties of active solids, self-oscillations are vital for biological systems such as flagella and cilia [21–23] and offer the prospect of autonomous mechanical behaviors in designer materials [18,19,24]. It is now well established that one-dimensional active chains exhibit flagellar motion: on the one hand, experimental studies have reported self-oscillatory behavior and synchronization in biological and colloidal systems [25–30]; on the other hand, theoretical and numerical studies have suggested that self-oscillations emerge from the competition between activity and elasticity [21–23,26,31–43]. Despite these advances, there are as of yet few model experimental platforms in which the predicted bifurcation scenarios that lead to self-oscillations and synchronization can be verified.

Here, to investigate dynamical transitions in elastoactive solids, we construct the experimental setup for a simplest form of active solids by elastically constraining centimeter-sized active particles in one-dimensional chains that can freely oscillate in the 2D plane. By controlling the elasticity of such structures, we uncover the nature of the transition to self-oscillations and synchronization. We find the transition to flagellar and self-snapping motion is governed by a nonlinear feedback between the direction of the active forces and the nonlinear elastic deflections. We find that synchronization between two elastoactive chains is mediated by elastically driven alignment, in contrast with active fluids. Although our proposed experimental platform is macroscopic, it might nonetheless help to advance our understanding of elastoactive instabilities that occur at the smaller scale in biological solids. We further envision that it will provide design guidelines for autonomous behaviors in active solids [44,45].

Experimental design of active chains.—Our system consists of $N = 75$ cm commercial self-propelled microbots (Hexbug Nano v2) [8,46] elastically coupled by a laser-cut silicon rubber chain pinned at one end as shown in Figs. 1(a) and 1(b) [47]. By tuning the width of the connection [W in Fig. 1(c)], we are able to manipulate the stiffness of the chain. When constrained at zero velocity, the microbot exerts a force in the direction of its polarization which is parallel to the chain's axis at rest and point in the same direction, toward the anchor point of the chain [Fig. 1(d)].

Transition to self-oscillations.—The chain with the largest width in between the active particles was slightly pushed off from the equilibrium and stayed at the same position without further significant movements as shown in Fig. 1(e). We then gradually reduced the width of the connections, at $W = 4.25 \pm 0.1$ mm, the self-oscillation behavior started to emerge [Fig. 1(f)] suggesting a competition between activity and elasticity: active forces from active particles destabilize the elastic chain, which in turn, through deformation, reorient the polarization of the
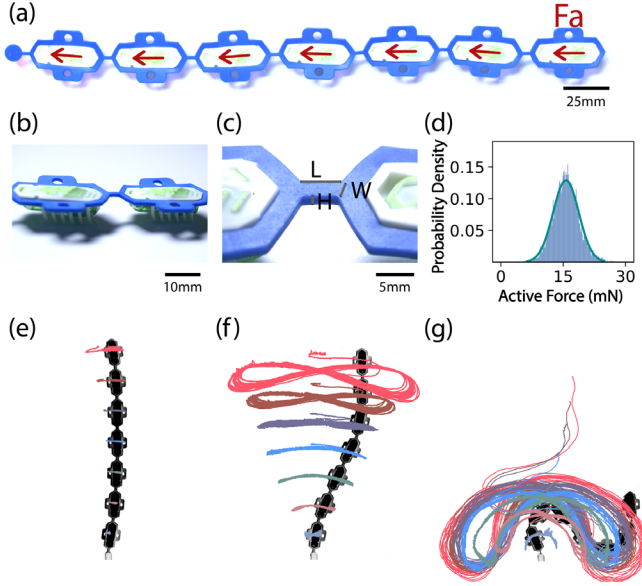
FIG. 1. Emergence of self-oscillations in elastoactive chains. (a) Configurations of seven active particles connected by a flexible rubber chain. (b) Close-up details of two active particles unveiling the design of the microbot. (c) A close-up of the linkage between each particle with width (W), thickness (H) and length (L). (d) Histogram of the active force measurements conducted at 0.05 mm/ min. (e),(f) Snapshots of the trajectories of the active particles showing the oscillations changed from self-amplified to overdamped with $W = 5$ mm, 4.4 mm, and 2 mm corresponding to elastoactive number $\sigma = 0.17$, 0.21, and 0.80, respectively. See also Videos in Supplemental Material [47].

FIG. 2. Characterization of the dynamics of elastoactive chains. (a) Snapshot of the elastoactive chain with $W = 17.7$ mm during its self-oscillation. (b) Time series of the angle between the first and last particle (mean polarization) was one of the parameters we chose to characterize the system, blue and orange represent the $\sigma = 0.695$ and $\sigma = 0.166$ chain, respectively. With the average of tangential angles of the particles (mean curvature) being the other parameter, plotting mean polarization (Θ) against mean curvature (Ω) gives (c) limit cycle showing that active forces balance with dissipation toward stable self-oscillation. (d) Schematics of an elastoactive chain of seven pendulums with active forces. (e),(f) Simulation results at $\sigma = 0.8$ showing good agreement with the experimental results.

particle, ultimately leading to self-oscillation. The magnitude of the oscillations increases drastically [shown in Fig. 1(g)] with decreasing W thanks to the competition between buckling and active force. This oscillatory dynamics can be quantified by the mean curvature $\Theta(t) := \sum_{i=1}^{N-1} \theta_{i+1}(t) - \theta_i(t) = \theta_7 - \theta_1$ and the mean polarization $\Omega(t) := (1/N) \sum_{i=1}^{N} \theta_i(t)$, where $\theta_i(t)$ is the instantaneous orientation of particle i with respect to the vertical axis [Figs. 2(a) and 2(b)]. While chains with large W come to a standstill, softer chains exhibit a limit cycle [Fig. 2(c)]. The area of this limit cycle arises directly from a balance of energy injection with dissipation.

Active pendulums model.—What is the origin of such transition? Inspired by the Ziegler destabilization paradox in structural mechanics [52–55] and the existing numerical models of active filaments [48,56–58], we construct a discrete model, where we boil the complexity of the elastic interactions down to three-body bending forces between the particles and the complexity of the vibration-induced dynamics to viscous overdamped dynamics. The discrete model is based on a chain of seven pendulums [shown as Fig. 2(d)] with one end fixed. The pendulums have a length ℓ and are connected to their neighbors via a torsional spring of torsional stiffness C. Each pendulum i is driven by a constant active force $\mathbf{F_i^a} = -F^a(\cos\theta_i \mathbf{e_x} + \sin\theta_i \mathbf{e_y})$ exerted on its

end and in the direction of the pendulum. We also introduce isotropic viscosity γ contributing to a dissipative force on the end of each pendulum that is only dependent on its velocity, and assume no inertia in the system [59]. We then collected all the terms in $\delta\theta_i$ for each i according to virtual-work theorem and constructed N nonlinear coupled differential algebraic equations (DAEs) that describe the motion of the elastoactive chain (further details in Supplemental Material [47]). There $\sigma = F^a\ell/C$ is the elastoactive parameter and $\tau = \gamma\ell^2/C$ a characteristic timescale. We estimate the torsional stiffness C from their geometry using beam theory (see Supplemental Material [47]). From the average velocity of the robots when they are freely moving $v_\mathbf{a} = 0.025 \pm 0.005$ m/s and their average force when they are pinned $F_\mathbf{a} = 15.7 \pm 3.1$ mN [Fig. 1(d)], we estimate the damping coefficient $\gamma = F_\mathbf{a}/v_\mathbf{a} = 0.63 \pm 0.11$ N s/m.

Using these parameters, we solve the system of DAEs numerically (see Supplemental Material [47]) and find a good agreement with the experimental results, and for the time series of average polarization [Fig. 2(e)]. We observe an agreement between the experiments and the simulation in the trend of the limit cycle [Fig. 2(f)], here the differences are due to the energy loss in the experimental scenarios. This agreement shows that nonlinear geometry, torsional stiffness, active force, and isotropic viscous dissipation are sufficient ingredients to successfully capture the essence of the self-oscillation phenomenon. Our elastoactive model is controlled by a single timescale τ and a single nondimensional
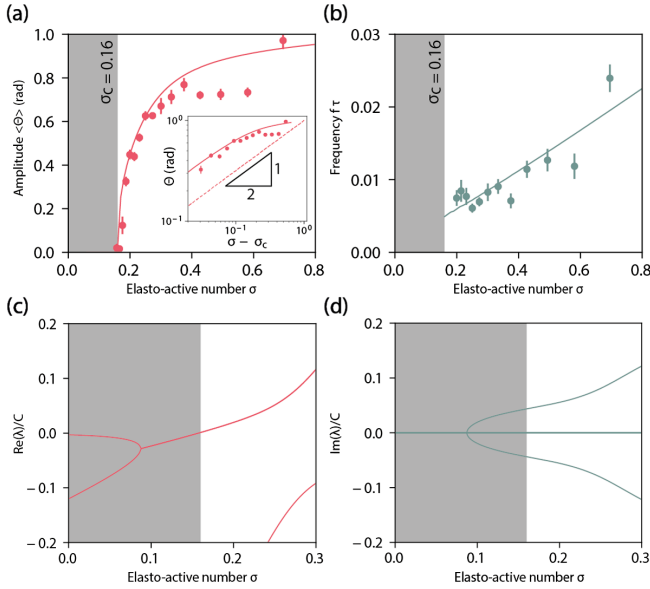
FIG. 3. An active system featuring a Hopf bifurcation at $\sigma = 0.15$. Simulation and experimental results showing the evolution of (a) amplitude and (b) frequency with increasing σ, respectively, for the chain with $N = 7$. The inset in (a) is a log-log plot demonstrating the power law between Θ and σ. (c) Real and imaginary (d) part of the eigenvalues of the Jacobian of Eqs. (1) and (2) vs elastoactive number σ for a minimal chain with $N = 2$. In all panels, the gray area represents the stable region.

parameter σ, which will allow us to probe the nature of the transition to self-oscillations in the following.

Supercritical Hopf bifurcation.—We ran experiments and simulations over a wide range of the elastoactive parameter σ, collected the time average of the amplitudes $\langle\Theta\rangle$ [Fig. 3(a)] and the rescaled oscillation frequency $f \times \tau$ [Fig. 3(b)] in the mean polarization time series and plotted them against elastoactive parameter σ. While for low values of σ, the chain remains straight without oscillations, we see that above a critical value $\sigma_c = 0.16 \pm 0.005$, the oscillation amplitude $\langle\Theta\rangle$ increases rapidly as $\langle\Theta\rangle \sim (\sigma - \sigma_c)^{0.5}$ [Fig. 3(a), inset], while the rescaled frequency increases linearly. To further elucidate the nature of the transition to self-oscillations, we carry out a linear stability analysis on the set of nonlinear coupled equations (see Supplemental Material [47]), and observe that at $\sigma = 0.15$, the real part of a pair of eigenvalues becomes positive, while the corresponding imaginary parts of these eigenvalues are equal and opposite and monotonically increase [Figs. 3(c) and 3(d)]. This transition is a hallmark of a Hopf bifurcation. The critical elastoactive number decreases with the length of the chain as $\sim 1/N^3$, See Supplemental Material [47] for simulations and theory, this can be interpreted by two effects: the Euler buckling load decreases for longer chains $\sim 1/N^2$ while the sum of the active forces grows as N. The exponent 0.5 in the experimental and numerical data suggests that this bifurcation is supercritical. To verify the nature of the bifurcation theoretically, we restrict our

attention to two pendulums with $N = 2$, which is the simplest case where the model could exhibit the bifurcation. The time evolution of such an elastoactive chain is governed by the following equations

$$\tau[2\dot{\theta}_1 + \dot{\theta}_2 \cos(\theta_1 - \theta_2)] = \theta_2 - 2\theta_1 + \sigma \sin(\theta_1 - \theta_2), \quad (1)$$

$$\tau[\dot{\theta}_1 \cos(\theta_1 - \theta_2) + \dot{\theta}_2] = \theta_1 - \theta_2. \quad (2)$$

In Supplemental Material [47], we use a perturbative expansion and perform a few algebraic manipulations to demonstrate that Eqs. (1) and (2) can be mapped onto the Landau-Stuart equation

$$\frac{dz}{dt} = (i + \sigma - 3)z + \left[i\left(\frac{17}{4} - \sigma\right) - \left(\sigma - \frac{5}{2}\right)\right]|z|^2 z, \quad (3)$$

where z is the complex variable defined by $z := \theta_1 + i\sqrt{(\sigma - 2)/(4 - \sigma)}\theta_2$. This equation is the canonical form of a supercritical Hopf bifurcation. Many earlier works had observed experimentally or numerically self-oscillation phenomena [21,25,60] or theoretically proposed models with Hopf bifurcations [23,31,32,35,48,61]; here, we unambiguously demonstrate experimentally, numerically, and theoretically in a single system of active chains that the supercritical Hopf bifurcation underlies the transition to self-oscillations and is primarily controlled by the elastoactive number σ.

Self-snapping.—When experimenting with the elastoactive chain, we realized that not only does it oscillate when pinned at one end, it also does oscillate when pinned at two ends, Fig. 4(a). We find that these oscillations vanish when the chain is maintained at its undeformed length, but that they immediately emerge once we compress the chain along its axis. A passive chain would simply buckle, i.e., bend sideways when compressed. In stark contrast, the elastoactive chain bends sideways, but continuously snaps by itself from one side to the other. The more the chain is compressed, the more it oscillates [Fig. 4(c)] and the slower it self-snaps [Fig. 4(d)]. We find that adding geometrical constraints to our model (see Supplemental Material [47]) allows us to reproduce the phenomenology qualitatively [Fig. 4(b)] [62]. While the flagellar motion observed earlier is ubiquitous in the context of biological structures, this self-snapping oscillation of buckled elastoactive structures is much more rare and surprising.

Frequency entrainment synchronization transition.—Our model system also allows us to explore synchronization phenomena between two active chains [Figs. 5(a)–5(d)]. We demonstrate experimentally and numerically that an elastic coupling allows for a frequency entrainment synchronization transition. We selected two chains both with an elastoactive number $\sigma_1 = 0.8$ [the chain on the left hand side in Fig. 5(a)] and an elastoactive number $\sigma_2 = 0.6$ [the chain on the right hand side in Fig. 5(a)] and connected
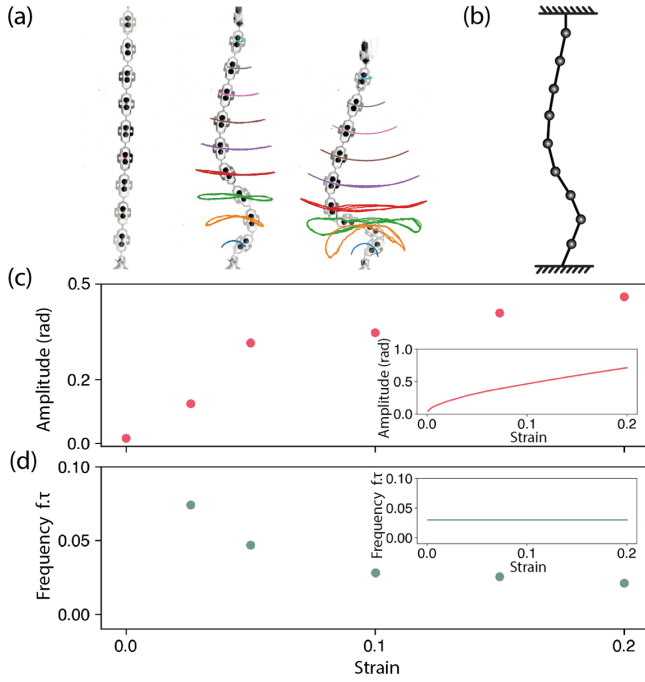
FIG. 4. Elastoactive chains pinned at both ends. Stills of an active chain where both ends are pinned with overlaid trajectories of the Hexbugs. The end-to-end distance between the pinning points is $\ell = 500$ mm (left), $\ell = 475$ mm (middle), and $\ell = 400$ mm (right). The length of the undeformed chain is $L = 500$ mm. (b) Model: sketch of the chain pinned at both ends. (c) Amplitude and (d) frequency of the self-snapping oscillations vs the compressive strain $(L - \ell)/L$. The insets are the corresponding data from the numerical model defined in Supplemental Material [47]. The elastoactive number of the chain is $\sigma = 0.8$. See also Videos in Supplemental Material [47].

them via a coupling spring of variable stiffness K. We also performed simulations over a range of stiffness K that contains what we have utilized in the experiments [Figs. 5(e) and 5(f)]. The rescaled coupling stiffness is $\kappa := K\ell^2/C_1$ (where C_1 is the stiffness of the left chain). To analyze the synchronization transition, we first extracted the oscillation signals from both chains. We then calculated the instantaneous phases $\Phi_1(t)$ and $\Phi_2(t)$ (see Supplemental Material [47]) of each time series [Figs. 5(b) and 5(e) for experiments and simulations, respectively]. For low coupling stiffness (yellow lines), both $\Phi_1(t)$ and $\Phi_2(t)$ increase linearly, but with a different slope, which can be described as two chains oscillating with different frequencies. On the contrary, for large coupling stiffness (brown lines), both instantaneous phases $\Phi_1(t)$ and $\Phi_2(t)$ align on the lowest slope (i.e., both chains beat at the lowest frequency of the two). We performed experiments and numerical simulations and measured the frequency mismatch $\delta\nu$ from the slope of the instantaneous phase difference $\Psi := \Phi_2(t) - \Phi_1(t)$ over a wide range of coupling stiffness and found that the synchronization transition occurs at the critical value $\kappa = 1.1$ [Figs. 5(c) and 5(f)] [63]. Further numerical
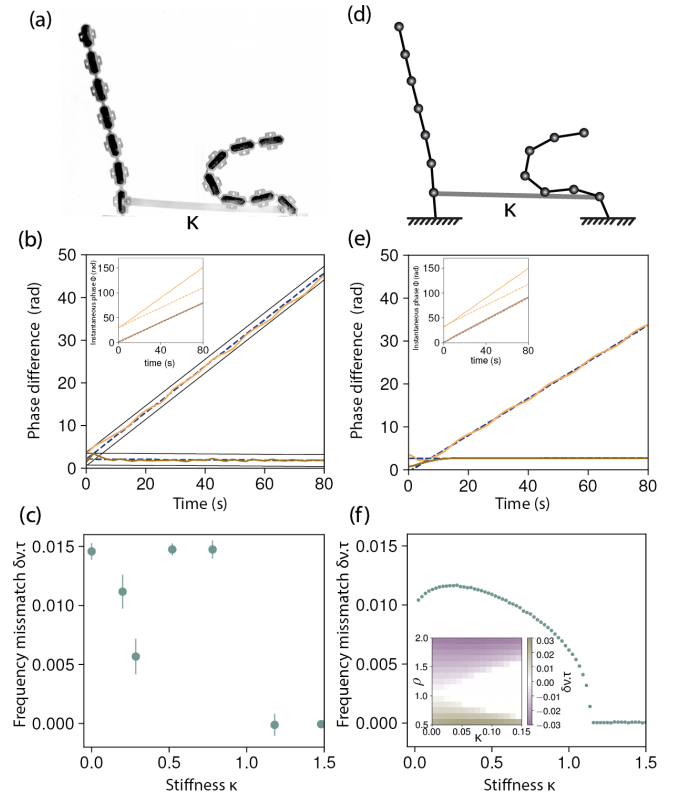
FIG. 5. Synchronization of two elastoactive chains with different elasticity coupled by the first particles only. (a) Snapshot of a pair of elastoactive chains with different elasticity coupled by another stiff silicon rubber chain. (b) Evolution of the instantaneous phase differences [instantaneous phases Φ_1 (dashed lines) and Φ_2 (solid lines) in inset] of two elastoactive chains with coupling strength $K = 0.8$ (yellow lines) and $K = 1.2$ (brown lines). (c) Instantaneous frequency difference extracted from the instantaneous phase difference Ψ vs rescaled coupling stiffness κ, with error bars corresponding to deviations on the linear regression [dashed blue line and black lines in panel (b)]. (d) Schematics of the numerical model adding a coupling spring (K) to two previously established elastoactive chains. (e),(f) Same data as (b),(c) for the numerical simulations. An Arnold tongue is observed when the frequency mismatch is plotted against the ratio between both elastoactive numbers ρ and the stiffness κ [inset of panel (f)].

simulations of elastoactive chains with varying σ reveal that the regime of synchronization exhibits an Arnold tongue centered about the 1:1 frequency ratio in the synchronization regime [Fig. 5(f), inset]. In other words, the two chains will synchronize for lower coupling if they have similar elastoactive numbers or if they are closer to the bifurcation—in this case the transition toward steady oscillatory synchronized state will take longer.

To rationalize this finding, we show in Supplemental Material [47] that the instantaneous phase difference $\Psi(t)$ between two chains with $N = 2$ is

$$\frac{d\Psi}{dt} = d\nu - \frac{\varepsilon}{\cos\Psi_0}\sin(\Psi - \Psi_0), \qquad (4)$$

where $d\nu$, ε, and Ψ_0 are functions of the elastoactive number of each chain and of the coupling stiffness between the chains (see Supplemental Material [47] for closed forms). This equation has been well studied before for the investigation of synchronization phenomena [64]. An analysis of this equation predicts synchronization for $|\varepsilon/\cos\psi_0| > |d\nu|$, with a square root singularity [64]. As we show in Supplemental Material [47], this condition is met when the coupling stiffness exceeds the threshold value $\kappa_c = 11/(4\sqrt{6})\sqrt{(\sigma-3)|1-\rho|}$, where σ is the elastoactive number of the left chain and where ρ is the ratio between the elastoactive number of the right chain over that of the left chain. This result thus demonstrates that the synchronization scenario of the two elastoactive chains corresponds to that of a classic nonisochronous synchronization, which is characterized by a constant phase shift in the synchronized region. In addition, the two chains will synchronize for lower coupling if they are closer to the bifurcation or when they have similar elastoactive numbers. In summary, we have captured experimentally, numerically, and analytically the synchronization transition of two elastically coupled active chains.

Conclusion.—In conclusion, we have shown that elastoactive chains exhibit transitions to self-oscillations and synchronization. Since they exhibit a nonlinear dynamics that is governed by activity, elasticity, and viscous damping, our study establishes macroscopic active structures as a powerful tool to investigate dynamical and autonomous behavior of active solids and living matter that exhibit collective self-oscillation at the microscale. Finally, fascinating future research directions could be taken from the minimalistic system considered here. For instance, one could investigate more complex geometries, such as nonfollower forces [44], more intricate geometrical connections between active particles, two-dimensional structures, alternative boundary conditions—pinned or moving clamping points (see Supplemental Material [47])—or even mechanical responses such as longitudinal or transverse excitations. These could in particular emulate peculiar dynamics observed in other contexts, such as odd elasticity [19] or the non-Hermitian skin effect [18,65].

[1] S. Saha, R. Golestanian, and S. Ramaswamy, Clusters, asters, and collective oscillations in chemotactic colloids, Phys. Rev. E **89**, 062316 (2014).

[2] M. C. Marchetti, J. F. Joanny, S. Ramaswamy, T. B. Liverpool, J. Prost, Madan Rao, and R. Aditi Simha, Hydrodynamics of soft active matter, Rev. Mod. Phys. **85**, 1143 (2013).

[3] S. Ramaswamy, Active matter, J. Stat. Mech. (2017) 054002.

[4] C. Bechinger, R. Di Leonardo, H. Löwen, C. Reichhardt, G. Volpe, and G. Volpe, Active particles in complex and crowded environments, Rev. Mod. Phys. **88**, 045006 (2016).

[5] J. Deseigne, O. Dauchot, and H. Chate, Collective Motion of Vibrated Polar Disks, Phys. Rev. Lett. **105**, 098001 (2010).

[6] C. A. Weber, T. Hanke, J. Deseigne, S. Léonard, O. Dauchot, E. Frey, and H. Chaté, Long-Range Ordering of Vibrated Polar Disks, Phys. Rev. Lett. **110**, 208001 (2013).

[7] A. Bricard, J.-B. Caussin, N. Desreumaux, O. Dauchot, and D. Bartolo, Emergence of macroscopic directed motion in populations of motile colloids, Nature (London) **503**, 95 (2013).

[8] O. Dauchot and V. Demery, Dynamics of a Self-Propelled Particle in a Harmonic Trap, Phys. Rev. Lett. **122**, 068002 (2019).

[9] T. Vicsek and A. Zafeiris, Collective motion, Phys. Rep. **517**, 71 (2012).

[10] A. Baskaran and M. C. Marchetti, Statistical mechanics and hydrodynamics of bacterial suspensions, Proc. Natl. Acad. Sci. U.S.A. **106**, 15567 (2009).

[11] D. Saintillan and M. J. Shelley, Active suspensions and their nonlinear models, C. R. Phys. **14**, 497 (2013).

[12] P. Reimann, Brownian motors: Noisy transport far from equilibrium, Phys. Rep. **361**, 57 (2002).

[13] W. F. Paxton, K. C. Kistler, C. C. Olmeda, A. Sen, S. K. St. Angelo, Y. Cao, T. E. Mallouk, P. E. Lammert, and V. H. Crespi, Catalytic nanomotors: Autonomous movement of striped nanorods, J. Am. Chem. Soc. **126**, 13424 (2004).

[14] J. R. Howse, R. A. L. Jones, A. J. Ryan, T. Gough, R. Vafabakhsh, and R. Golestanian, Self-Motile Colloidal Particles: From Directed Propulsion to Random Walk, Phys. Rev. Lett. **99**, 048102 (2007).

[15] E. Lauga and T. R. Powers, The hydrodynamics of swimming microorganisms, Rep. Prog. Phys. **72**, 096601 (2009).

[16] W. C. K. Poon, From *Clarkia* to *Escherichia* and Janus: The physics of natural and synthetic active colloids, Proc. Int. Sch. Phys. Enrico Fermi **184**, 317 (2013).

[17] R. J. Hawkins and T. B. Liverpool, Stress Reorganization and Response in Active Solids, Phys. Rev. Lett. **113**, 028102 (2014).

[18] M. Brandenbourger, X. Locsin, E. Lerner, and C. Coulais, Non-reciprocal robotic metamaterials, Nat. Commun. **10**, 4608 (2019).

[19] Colin Scheibner, Anton Souslov, Debarghya Banerjee, P. Surówka, W. T. M. Irvine, and V. Vitelli, Odd elasticity, Nat. Phys. **16**, 475 (2020).

[20] Y. Ozkan-Aydin, D. I. Goldman, and M. S. Bhamla, Collective dynamics in entangled worm and robot blobs, Proc. Natl. Acad. Sci. U.S.A. **118**, e2010542118 (2021).

[21] K. E. Machin, Wave propagation along flagella, J. Exp. Biol. 35, 796 (1958).

[22] C. J. Brokaw, Molecular mechanism for oscillation in flagella and muscle, Proc. Natl. Acad. Sci. U.S.A. 72, 3102 (1975).

[23] S. Camalet, F. Jülicher, and Jacques Prost, Self-Organized Beating and Swimming of Internally Driven Filaments, Phys. Rev. Lett. 82, 1590 (1999).

[24] F. G. Woodhouse, H. Ronellenfitsch, and J. Dunkel, Autonomous Actuation of Zero Modes in Mechanical Networks Far from Equilibrium, Phys. Rev. Lett. 121, 178001 (2018).

[25] D. Nishiguchi, J. Iwasawa, H.-R. Jiang, and M. Sano, Flagellar dynamics of chains of active Janus particles fueled by an ac electric field, New J. Phys. 20, 015002 (2018).

[26] K. Y. Wan, K. C. Leptos, and R. E. Goldstein, Lag, lock, sync, slip: The many "phases" of coupled flagella, J. R. Soc. Interface 11, 20131160 (2014).

[27] W. Zhou, Z. Hao, and N. Gravish, Collective Synchronization of Undulatory Movement through Contact, Phys. Rev. X 11, 031051 (2021).

[28] D. R. Brumley, K. Y. Wan, M. Polin, and R. E. Goldstein, Flagellar synchronization through direct hydrodynamic interactions, eLife 3, e02750 (2014).

[29] R. E. Goldstein, M. Polin, and I. Tuval, Emergence of Synchronized Beating during the Regrowth of Eukaryotic Flagella, Phys. Rev. Lett. 107, 148103 (2011).

[30] R. K. Manna, P. B. Sunil Kumar, and R. Adhikari, Colloidal transport by active filaments, J. Chem. Phys. 146, 024901 (2017).

[31] A. Hilfinger and F. Jülicher, The chirality of ciliary beats, Phys. Biol. 5, 016003 (2008).

[32] A. Hilfinger, A. K. Chattopadhyay, and F. Jülicher, Nonlinear dynamics of cilia and flagella, Phys. Rev. E 79, 051918 (2009).

[33] H. C. Fu, C. W. Wolgemuth, and T. R. Powers, Beating patterns of filaments in viscoelastic fluids, Phys. Rev. E 78, 041913 (2008).

[34] J. Gladrow, C. P. Broedersz, and C. F. Schmidt, Nonequilibrium dynamics of probe filaments in actin-myosin networks, Phys. Rev. E 96, 022408 (2017).

[35] R. Chelakkot, A. Gopinath, L. Mahadevan, and M. F. Hagan, Flagellar dynamics of a connected chain of active, polar, Brownian particles, J. R. Soc. Interface 11, 20130884 (2014).

[36] G. Quaranta, M.-E. Aubin-Tam, and D. Tam, Hydrodynamics Versus Intracellular Coupling in the Synchronization of Eukaryotic Flagella, Phys. Rev. Lett. 115, 238101 (2015).

[37] K. Y. Wan and R. E. Goldstein, Coordinated beating of algal flagella is mediated by basal coupling, Proc. Natl. Acad. Sci. U.S.A. 113, E2784 (2016).

[38] T. Niedermayer, B. Eckhardt, and P. Lenz, Synchronization, phase locking, and metachronal wave formation in ciliary chains, Chaos 18, 037128 (2008).

[39] B. Guirao and J.-F. Joanny, Spontaneous creation of macroscopic flow and metachronal waves in an array of cilia, Biophys. J. 92, 1900 (2007).

[40] G. Jayaraman, S. Ramachandran, S. Ghose, A. Laskar, M. Saad Bhamla, P. B. Sunil Kumar, and R. Adhikari, Autonomous Motility of Active Filaments due to Spontaneous Flow-Symmetry Breaking, Phys. Rev. Lett. 109, 158302 (2012).

[41] R. R. Bennett and R. Golestanian, Emergent Run-and-Tumble Behavior in a Simple Model of Chlamydomonas with Intrinsic Noise, Phys. Rev. Lett. 110, 148102 (2013).

[42] A. Vilfan and F. Jülicher, Hydrodynamic Flow Patterns and Synchronization of Beating Cilia, Phys. Rev. Lett. 96, 058102 (2006).

[43] G. De Canio, E. Lauga, and R. E. Goldstein, Spontaneous oscillations of elastic filaments induced by molecular motors, J. R. Soc. Interface 14, 20170491 (2017).

[44] P. Baconnier, D. Shohat, C. Hernández López, C. Coulais, V. Démery, G. Düring, and O. Dauchot, Selective and collective actuation in active solids, Nat. Phys. 18, 1234 (2022).

[45] M. Brandenbourger, C. Scheibner, J. Veenstra, V. Vitelli, and C. Coulais, Active impact and locomotion in robotic matter with nonlinear work cycles, arXiv:2108.08837.

[46] D. L. Christensen, S. A. Suresh, K. Hahm, and M. R. Cutkosky, Let's all pull together: Principles for sharing large loads in microrobot teams, IEEE Rob. Autom. Lett. 1, 1089 (2016).

[47] See Supplemental Material at http://link.aps.org/supplemental/10.1103/PhysRevLett.130.178202 for simulations and theory, which includes Refs. [35,38,43,48–51]. The precise number of particles N, which does not affect the bifurcation phenomena, was chosen because of experimental considerations such as manufacturing and visualization. In addition, we also ran an additional experiment $N = 17$, which displays the same self-oscillating pattern. Finally, we performed a linear stability analysis, which also demonstrates that the unstable mode does not depend on system size.

[48] K. Sekimoto, N. Mori, K. Tawada, and Y. Y. Toyoshima, Symmetry Breaking Instabilities of an In Vitro Biological System, Phys. Rev. Lett. 75, 172 (1995).

[49] W. C. Young, R. G. Budynas, Ali M. Sadegh et al., Roark's Formulas for Stress and Strain (McGraw-Hill, New York, 2002), Vol. 7.

[50] https://www.math.arizona.edu/~lega/454/Fall06/Hopf_Bifurcation.pdf.

[51] J. Guckenheimer and P. Holmes, Nonlinear Oscillations, Dynamical Systems, and Bifurcations of Vector Fields, Applied Mathematical Sciences (Springer, New York, 1983).

[52] F. Bosi, D. Misseroni, F. Dal Corso, S. Neukirch, and D. Bigoni, Asymptotic self-restabilization of a continuous elastic structure, Phys. Rev. E 94, 1 (2016).

[53] P. Hagedorn, On the destabilizing effect of nonlinear damping in non-conservative systems with follower forces, Int. J. Nonlinear Mech. 5, 341 (1970).

[54] D. Bigoni and G. Noselli, Experimental evidence of flutter and divergence instabilities induced by dry friction, J. Mech. Phys. Solids 59, 2208 (2011).

[55] H. Ziegler, Die Stabilitätskriterien der Elastomechanik, Ingenieur-Archiv 20, 49 (1952).

[56] Z. Farkas, I. Derényi, and T. Vicsek, Dynamics of Actin Filaments in Motility Assays, Struct. Dyn. Confined Polymers 327 (2002), 10.1007/978-94-010-0401-5_20.

[57] R. E. Isele-Holder, J. Elgeti, and G. Gompper, Self-propelled worm-like filaments: Spontaneous spiral formation, structure, and dynamics, Soft Matter **11**, 7181 (2015).

[58] R. G. Winkler, J. Elgeti, and G. Gompper, Active polymers—Emergent conformational and dynamical properties: A brief review, J. Phys. Soc. Jpn. **86**, 1 (2017).

[59] A more accurate description would include additional effects such as noise in the active force and anisotropic viscous drag. In the former case, the noise is multiplicative in the equations of motion, which in turn progressively introduces noise to the trajectory of the active chain as the noise of the active force is increased; see Supplemental Material [47].

[60] C.-J. Lo, Y. Sowa, T. Pilizota, and R. M. Berry, Mechanism and kinetics of a sodium-driven bacterial flagellar motor, Proc. Natl. Acad. Sci. U.S.A. **110**, E2544 (2013).

[61] S. Gonzalez and R. Soto, Active colloidal chains with Cilia- and Flagella-like motion, New J. Phys. **20**, 053014 (2018).

[62] We find that the model overestimates the magnitude of oscillations by a factor 2 and that it fails to capture the decrease of self-snapping frequency as the chains is more compressed. We attribute the discrepancy between the experiment and the model to the fact we assumed the friction to be isotropic. In reality, the lateral drag is much larger than the longitudinal drag and this simplifying hypothesis can plausibly lead to predictions that overestimate the magnitude and the frequency of snapping.

[63] For the experimental results, the dip in the frequency miss-match at intermediate stiffness is due to friction effect that could not be avoided for small beam stiffness.

[64] A. Pikovsky, M. Rosenblum, and J. Kurths, *Synchronization: A Universal Concept in Nonlinear Science* (Cambridge University Press, New York, 2002).

[65] C. Coulais, R. Fleury, and J. van Wezel, Topology and broken Hermiticity, Nat. Phys. **17**, 9 (2020).

[66] E. Zheng, M. Brandenbourger, L. Robinet, P. Schall, E. Lerner, and C. Coulais, Data set for the article "Self-oscillation and Synchronisation Transitions in Elasto-Active Structures" (2022), 10.5281/zenodo.6549887.